THE JOURNAL OF PHYSICAL CHEMISTRY B

Article

pubs.acs.org/JPCB

Ionic Conductivity of Mixed Glass Former $0.35Na_2O + 0.65[xB_2O_3 + (1 - x)P_2O_5]$ Glasses

Randilynn Christensen,† Garrett Olson, and Steve W. Martin*

Department of Materials Science and Engineering Iowa State University, Ames, Iowa 50011

ABSTRACT: The mixed glass former effect (MGFE) is defined as a nonlinear and nonadditive change in the ionic conductivity with changing glass former fraction at constant modifier composition between two binary glass forming compositions. In this study, mixed glass former (MGF) sodium borophosphate glasses, $0.35Na_2O + 0.65[xB_2O_3 + (1 - x)P_2O_5]$, $0 \leq x \leq 1$, have been prepared, and their sodium ionic conductivity has been studied. The ionic conductivity exhibits a strong, positive MGFE that is caused by a corresponding strongly negative nonlinear, nonadditive change in the conductivity activation energy with changing glass former content, x. We describe a successful model of the MGFE in the conductivity activation energy terms of the underlying short-range order (SRO) phosphate and borate glass former structures present in these glasses. To do this, we have developed a modified Anderson-Stuart (A–S) model to explain the decrease in the activation energy in terms of the atomic level composition dependence (x) of the borate and phosphate SRO structural groups, the Na^+ ion concentration, and the Na^+ mobility. In our revision of the A–S model, we carefully improve the treatment of the cation jump distance and incorporate an effective Madelung constant to account for many body coulomb potential effects. Using our model, we are able to accurately reproduce the composition dependence of the activation energy with a single adjustable parameter, the effective Madelung constant, that changes systematically with composition, x, and varies by no more than 10% from values typical of oxide ceramics. Our model suggests that the decreasing columbic binding energies that govern the concentration of the mobile cations are sufficiently strong in these glasses to overcome the increasing volumetric strain energies (mobility) caused by strongly increasing glass-transition temperatures combined with strongly decreasing molar volumes of these glasses. The dependence of the columbic binding energy term on the relative high-frequency dielectric permittivity suggests that the increased polarizability of the bridging oxygens connecting SRO tetrahedral boron units to phosphorus units causes further charge delocalization away from the negatively charged tetrahedral boron units, leading to a lowering of the charge density, and is the underlying cause of the MGFE.

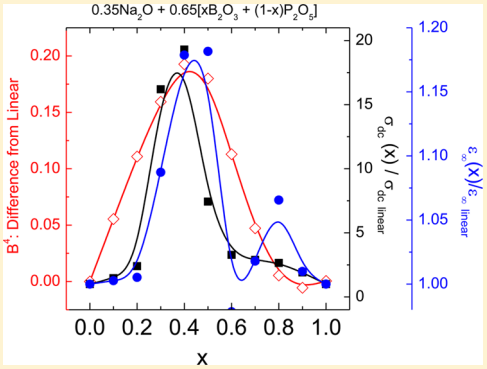

1. INTRODUCTION

1.1. Background. Energy storage is a growing concern in an ever increasingly portable-energy (battery)-driven society. Batteries power everything from cell phones to computers to medical devices to automobiles. The development of safer, smaller, and more energy-dense batteries is in demand. Ion-conducting glasses are an important type of solid electrolyte that may be used to answer this need.[1−7] A currently unexplained source of change in the ionic conductivity in glasses known as the mixed glass former effect (MGFE) has been seen in many mixed glass former (MGF) glasses[8−15] such as $Li_2S + GeS_2 + GeO_2$ glasses[16] and $Li_2S + SiS_2 + GeS_2$ glasses.[10] This change in the ionic conductivity is nonlinear and nonadditive and can be observed as either a decrease or an increase in the ionic conductivity with changing glass former fraction at constant modifier composition between the two binary glass forming systems. In some MGF glasses, like those to be described here, simultaneous to this exponential increase in the Na^+ ion conductivity is the corresponding improvement in the glass transition temperature (T_g), the improvement in the glass -forming ability, and the chemical durability of these glasses. Such simultaneous improvements in these important physical properties of these glasses with little to no negative changes in other properties make these MGF glassy electrolytes attractive as solid electrolytes for next-generation batteries. While this phenomena has not been fully explained,[9,10,14,17] increases in the ionic conductivity of up to two orders of magnitude have been observed in other MGF glasses reported in the literature.[8,9] Understanding the cause of the MGFE at the atomic structural level of glass is crucial to the effort of engineering glasses with higher ionic conductivities and other improved physical properties and is a key motivation for the present study.

To better understand the effect of composition on the Na^+ ion conductivity, the physical properties, and structures of these glasses, we carefully chose all components of the glasses in the present study. Oxygen was selected as the anion with Na, P, and B as the cations. Boron and phosphorus were chosen because of their nuclear magnetic resonance spectroscopy (NMR) accessible isotopes, ^{11}B and ^{31}P. Oxygen was

Received: September 23, 2013
Revised: November 28, 2013
Published: December 2, 2013

chosen as the anion because of the strong glass-forming ability of B_2O_3 and P_2O_5. Sodium was chosen as the glass modifier and ionic charge carrier because its radioactive isotope is useful for tracer diffusion measurements and ^{23}Na is useful in NMR studies.

The structures and physical properties, such as density, T_g, and ionic conductivity, of B_2O_3[18−20] and P_2O_5[21] glasses, their binary glassy counter parts, $Na_2O + B_2O_3$[20,22] and $Na_2O + P_2O_5$,[23−26] and some ternary alkali borophosphate glasses,[15,27−30] have been well-studied in the literature. The data reported in these literature works allow the experimental data of our glasses to be checked for accuracy and can be used as starting points for further analysis. It is recognized at the outset that these all-oxide glasses, even though being well "engineered" for this specific study of the MGFE, will nonetheless have relatively low Na^+ ion conductivities. It is our expectation, however, that through a detailed and well-designed study of these glasses the underlying mechanism of the MGFE in these glasses can be determined and modeled. Through such insight into the conduction mechanism in these glasses, it will be possible to advance the development of more highly conducting glasses, which may find application in advanced sodium batteries.

It is our hypothesis that structural changes in the short-range order (SRO), first-coordination sphere, and intermediate range order (IRO), second- and third-coordination spheres, caused by the mixing of the two glass former networks is the underlying cause of the MGFE. To confirm this hypothesis, we have explored the link between the physical properties, structures, and compositions of MGF glasses. The full results of the previous analyses on the structural and physical properties of our glasses can be seen in the works by Christensen et al.,[31−33] Le Roux et al.,[34] and Schuch et al.[35] A positive nonlinear, nonadditive, MGFE trend was observed in the density and T_g with changing glass former composition with a maxima at $x = 0.4$ in the glass series $0.35Na_2O + 0.65[xB_2O_3 + (1 - x)P_2O_5]$. The positive MGFE trend in the density of these glasses suggests that an MGFE in the ionic conductivity trend will also be observed. However, the free volume of the glasses was found to undergo a strongly negative nonlinear, nonadditive trend, with a minima at $x = 0.4$. This decrease in free volume suggests a decrease in ionic mobility, and a corresponding decrease in the ionic conductivity will be found. Similarly, the maximum in the T_g of these glasses suggests a maximum in the mechanical modulus of the glasses, and this effect would also predict a minimum in the ionic conductivity and a maximum in the conductivity activation energy. Despite the trends in the molar volume and the T_g, a positive MGFE is exhibited. For these reasons, these glasses are further advantageous to study because the observed positive MGFE suggests that whatever the cause it must be a strong function of composition. If understood, this cause could be a compositional and structural tool to produce glasses with even higher ionic conductivities.

Raman and NMR structural studies were used to create a quantitative SRO model. The complete results of this structural model can be found in our previous paper.[31] The distribution of sodium cations between boron and phosphorus oxy-anions was found to be unequal and changed with changing glass former composition. The sodium cations preferentially modified the majority glass former, modifying B in the $x = 0.1$ to 0.6 range and P in the $x = 0.7$ to 0.9 range. Thermodynamic modeling suggested that the large thermodynamic stability of the B^4 group drives the unequal sharing of the Na^+ ion. In addition, the changes in T_g were found to be directly proportional to the number of bridging oxygens (BOs) in the glasses and were driven by the concentration of the cross-linking (BO) effect of the B^4 SRO structural units in the glass. The results of the SRO model created by Raman and NMR structural studies was found to be in excellent agreement with the reverse Monte Carlo (RMC) model of these glasses created from X-ray diffraction (XRD) studies.[35] The RMC model also suggests a non-randomly connected network where B−O−P bonds are favored. It was also found that there is no correlation between the percolating accessible volume (volume available for sodium ion movement under the hard-sphere constraints of the model) and the activation energy of the ionic conductivity, suggesting that changes in the free volume available to the conducting ion may not be strongly influential to the activation energy. The ionic conductivity models of Anderson and Stuart[36] have been combined with our experimental ionic conductivity data to develop an atomic-level understanding of the positive MGFE in the Na^+ ion conductivity in these Na B P O glasses. In our model, we are able to show that the volumetric contributions are small and do not strongly influence the ionic activation energy, whereas the columbic contributions to the total activation energy are much larger and are the dominant cause of the MGFE in these glasses.

1.2. Glass Structure Notations. The SRO glass structures will be referred to as J_{mK}^{n}, where J is the glass former connected to n number of BOs, with m number of the BOs bonding to glass former K and n-m BOs going to glass former J. For example, P_{mB}^{n} indicates a phosphorus atom with n number of BOs that bond to m number of boron atoms and (n-m) number of phosphorus atoms. If no mK is denoted, then it is unknown what glass former is being bridged to by oxygen. The SRO structures present in the binary glasses and their approximate compositional ranges over which they are observed are shown in Figures 1 and 2.

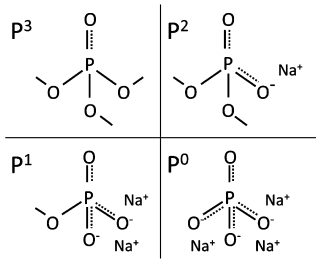

Figure 1. Binary sodium phosphate glass SRO structures, $yNa_2O + (1 - y)P_2O_5$. P^3 is present from $0 \leq y < 0.5$. P^2 is present from $0 < y < 0.65$. P^1 is present from $0.5 < y$. P^0 is present from $0.65 < y$.

2. EXPERIMENTAL METHODS

2.1. Sample Preparation. The starting materials were sodium carbonate (Na_2CO_3, 99.5% Fisher Scientific), ammonium hydrogen phosphate dibasic ($(NH_4)_2HPO_4$, 98.8% Fisher Scientific), and boric acid (H_3BO_3, 99.5% Fisher Scientific). After weighing and mixing the appropriate amounts, the starting materials were calcined in platinum crucibles between 900 and 1100 °C for 0.5 to 1 h in an

dx.doi.org/10.1021/jp409497z | J. Phys. Chem. B 2013, 117, 16577−16586

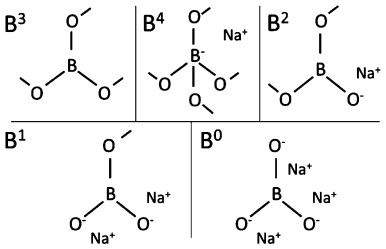

Figure 2. Binary sodium borate glass SRO structures, $yNa_2O + (1 - y)B_2O_3$. B^3 is present from $0 \leq y < 0.25$. B^4 is present from $0 < y$. B^2 is present from $0.3 < y < 0.7$. B^1 is present from $0.45 < y$. B^0 is present from $0.55 < y$.

electric furnace in a fume hood. After the melt was bubble-free, the crucible was removed from the furnace and allowed to cool to room temperature. Once cool, the sample was weighed to determine the weight lost from NH_3, H_2O, and CO_2. The slightly hygroscopic samples were then transferred to a high-quality nitrogen atmosphere glovebox (typically <5 ppm O_2 and H_2O) and remelted in an electric furnace at 1000−1100 °C for 10 min. To create bulk samples for conductivity measurements, the melt was quenched in preheated brass molds at temperatures 40 °C below the T_g of the glass. Bulk samples were cast as round discs ~20 mm in diameter and 2 mm thick. The bulk samples were annealed 40 °C below the T_g for 0.5 h, then cooled to room temperature at a rate of 2 °C/min. Because of their hygroscopic character, all samples were stored in the N_2 atmosphere glovebox. Selected compositions of the glasses were checked for crystallization with XRD and found to be X-ray amorphous. Samples were checked for weight loss and found to be within ±1.5 wt % of their target weight. Sodium, oxygen, and phosphorus concentrations were checked by energy-dispersive spectroscopy and found to be within ±4 at % of the target compositions. Infrared spectroscopy was used to ensure that all of the glasses did not contain residual NH_3, CO_2, and H_2O.

2.2. Ionic Conductivity. Bulk samples 20 mm in diameter and ~2 mm thick were polished using sandpapers and polishing cloths to 4000 grit to optical transparency and then sputtered with gold electrodes on both sides of the sample ~50 nm thick and 20 mm in diameter. Samples were measured from 0.01 Hz to 10 MHz in log 1.4 increments from 0 to 300 °C in 20 °C increments using a Novocontrol Concept 80 impedance spectrometer using 1 V rms. Complex plane impedance analysis of the impedance data, Figure 3, provides an example, and how the $\sigma_{dc}(T)$ was determined was used to extract the equivalent circuit dc resistance of the glasses as a function of temperature and composition.

3. RESULTS

An example of the ac ionic conductivity measurements over the temperature and frequency ranges that were performed on all the samples can be seen in a complex impedance plot for one glass, shown in Figure 3. The semicircle at high frequency arises from the bulk response of the glass to the applied electric field. The polarization "tail" at low frequency arises from the space-charge polarization effects of Na^+ ion accumulation at the sputtered gold-blocking electrodes. The equivalent circuit resistance (R) is equal to the real impedance (Z') when the imaginary impedance (Z'') is equal to zero. The bulk resistance, $R = Z'$, was obtained from the

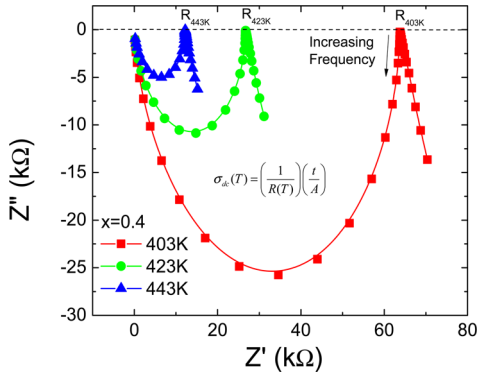

Figure 3. Example of real versus imaginary impedance plots of the $0.35Na_2O + 0.65[xB_2O_3 + (1 - x)P_2O_5]$ glasses at $x = 0.4$ composition at 403, 423, and 443 K.

intersection of the bulk response semicircle with the $Z'' = 0$ axis at low frequencies. The resistance was then used to calculate the dc conductivity, σ_{dc}, by using the cell constant of the prepared glasses samples, $\sigma_{dc} = (t/(R*A))$, where t = thickness, R = resistance, and A = area of the circular electrode.

The temperature dependencies of the ionic conductivities of the "even composition" glasses are shown in Figure 4 in the

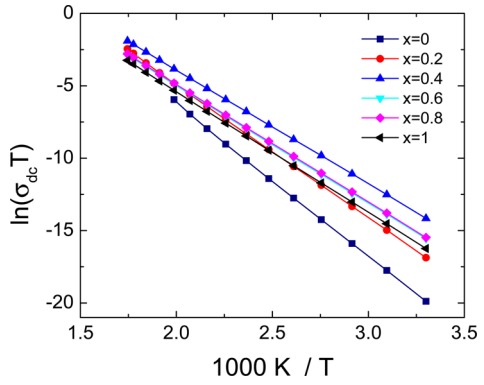

Figure 4. Example of the Arrhenius plots of the $0.35Na_2O + 0.65[xB_2O_3 + (1 - x)P_2O_5]$ glasses.

form of an Arrhenius plot. For all samples, the conductivity increases in an Arrhenius manner, ln σ_{dc} T versus $1/T$, from room temperature (T) to just below T_g. In one case, however, we explored the temperature dependence to much lower temperatures to more fully examine the non-Arrhenius behavior of the ionic conductivity; see later.

The activation energy of ionic conduction, ΔE_a, was calculated using eq 1.

$$\sigma_{dc}(T) = \frac{\sigma_0}{T} \exp\left(-\frac{\Delta E_a}{RT}\right) \quad (1)$$

where σ_{dc} is the direct current ionic conductivity, T is the temperature in Kelvin, ΔE_a is the activation energy of the Na^+ ion conduction, R is the gas constant, and σ_0 is the pre-exponential factor. The activation energy and the room-temperature conductivities for this glass series are given in Figure 5. The ionic conductivity of sodium phosphate glass at 30 °C at $x = 0$ is 7.63×10^{-12} $(ohm*cm)^{-1}$. With the addition of boron, the Na^+ ion conductivity increases to a maximum of 2.34×10^{-9} $(ohm*cm)^{-1}$ at $x = 0.4$. Further

dx.doi.org/10.1021/jp409497z | J. Phys. Chem. B 2013, 117, 16577−16586

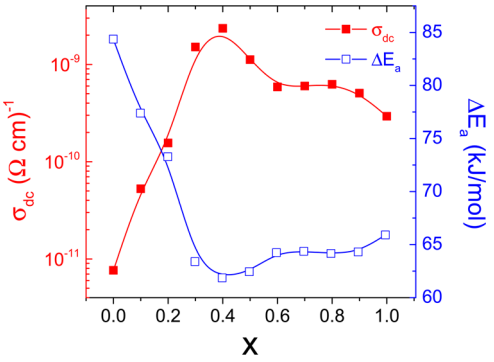

Figure 5. Ionic dc conductivity and activation energy of $0.35Na_2O + 0.65[xB_2O_3 + (1 - x)P_2O_5]$ glasses at 30 °C. Error bars are smaller than symbols.

additions of boron cause the conductivity to decrease to 5.86×10^{-10} $(ohm*cm)^{-1}$ at $x = 0.6$. The conductivity remains nearly constant through $x = 0.8$, then finally decreases to 2.93×10^{-10} $(ohm*cm)^{-1}$ in the pure sodium borate glass. As expected from eq 1, the activation energy has an opposing trend to the ionic conductivity. The maximum activation energy is 84.36 kJ/mol for the $x = 0$ glass. A decrease to 61.86 kJ/mol for the $x = 0.4$ glass is followed by an increase to 64.24 kJ/mol for the $x = 0.6$ glass. The activation energy remains nearly constant until it increases to 65.91 kJ/mol for the $x = 1$ glass. We next turn our attention to the atomic level understanding of the composition dependence of the activation energy and, in turn, the Na^+ ion conductivity.

3.1. Theory of Ionic Conductivity in the Glassy State.

3.1.1. Arrhenius Conductivity. In its most general form, the ionic conductivity of ion-conducting glasses is given by the relation $\sigma = nZe\mu$, where σ is the ionic conductivity, Z is the charge of the mobile ion ($^+1$ in the case of Na here), e is the electric charge, n is the number of mobile ions (Na^+) per unit volume, and μ is the mobility of the ions. Both n and μ are composition- and temperature- dependent through a corresponding Arrhenius relationship given in eqs 2 and 3.

$$n(T) = n_0 \exp\left(-\frac{\Delta E_n}{RT}\right) \tag{2}$$

$$\mu(T) = \frac{\mu_0}{T} \exp\left(-\frac{\Delta E_m}{RT}\right) \tag{3}$$

where n_0 and μ_0 are the total number density of cations in the glass and mobility pre-exponential factors, respectively. ΔE_n and ΔE_m are the activation energies for creating a mobile cation and for the mobility of the cation, respectively.

Combining eqs 1−3 shows that:

$$\Delta E_a = \Delta E_n + \Delta E_m \tag{4}$$

The two activation energies combine to form the total activation energy for ion conduction, eq 4. It is assumed that both ΔE_n and ΔE_m are not single valued but rather represent averages of the natural distributions of these energy barriers created through the structural disorder in glass. Such distributions would be expected to create a non-Arrhenius temperature dependence in the ionic conductivity, where the lower energy tail of the distribution would be more dominant at "lower" temperatures, the median values of the distribution would be more dominant at the "intermediate" temperatures, and the higher energy tail of the distribution would be dominant at the "higher" temperatures. The quotes are purposefully used here to denote the fact that as the average value of the energy distribution changes with changing glass composition to higher and lower values, these temperature ranges would, of course, in turn change to higher and lower values, respectively. However, this temperature dependence of the slope (activation energy) of the ionic conductivity is not observed in the data of Figure 4 over the range of temperatures used in this study, 0 to 300 °C. This finding is consistent with the behavior observed for nearly all oxide glasses studied in the literature to date, although some examples of non-Arrhenius behavior do exist.[37−39] However, in the more recent literature of more highly conducting (lower average activation energy) glasses, several instances of non-Arrhenius temperature dependence of the alkali ion conductivity in sulfide glasses can be found.[40−43] In most papers, the non-Arrhenius temperature dependence of the conductivity is often ignored, and it is often treated as a simple Arrhenius function, resulting in a single value for the activation energy, ΔE_a.

3.1.2. Non-Arrhenius Conductivity. Bischoff et al.,[44] from our laboratory, have suggested a resolution to this long-standing question of why simple Arrhenius-behaving conductivities are observed for the less conductive, higher average activation energy oxide glasses, whereas non-Arrhenius conductivities are more frequently observed in higher conducting, lower average activation energy sulfide glasses. These authors observed that for the most commonly measured temperature ranges, from room temperature to ~300 °C, the temperature dependence of the activation energy arising from a Gaussian distribution of activation energies (DAE) could be accurately approximated by the expression:

$$\langle \Delta E \rangle = \Delta E_0 - \frac{\delta^2}{RT} \tag{5}$$

where $\langle \Delta E \rangle$, the temperature dependent expectation energy for conduction, is used to replace the single-valued activation energy ΔE_a of Arrhenius-type conductivity. ΔE_0 is the mean value of the temperature-independent DAE, and δ is the standard deviation of the DAE. Hence, eq 5 shows that for large values of ΔE_0 and small values of δ, as appears to be the case for the vast majority of alkali ion conducting oxide glasses, a weak or barely observable non-Arrhenius temperature dependence of the ionic conductivity is expected in the range of temperatures from room to 300 °C.

However, Bischoff et. al's. eq 5 also shows that a non-Arrhenius dependence of the ionic conductivity would be more evident even with a large value of ΔE_0, as is the case for the glasses of the present study, if the ionic conductivity were measured at lower temperatures. For this reason, an additional study of the ionic conductivities in the 300 to −100 °C range was undertaken. The wider temperature range dependence of the conductivity of the $0.35\ Na_2O + 0.65\ [0.4B_2O_3 + 0.6P_2O_5]$ glass can be seen in Figure 6. The ionic conductivity was found to be more strongly non-Arrhenius over the expanded temperature range, where the slope decreases with decreasing temperatures, in the manner expected from the previous description. The nonlinearity of the conductivity is especially noticeable in the temperature range of 25 to −100 °C. From the best-fit of eq 5 to the conductivity data in Figure 6, the mean activation energy, ΔE_0, was found to equal 107 kJ/mol, and the standard deviation, δ, equals 7.793 kJ/

dx.doi.org/10.1021/jp409497z | J. Phys. Chem. B 2013, 117, 16577−16586

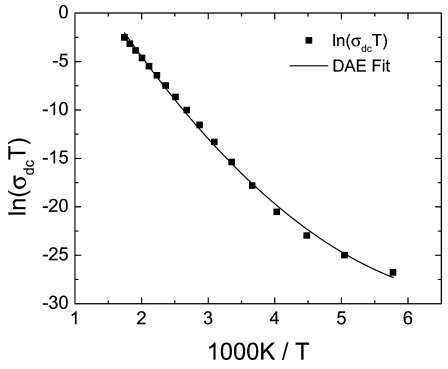

Figure 6. Non-Arrhenius temperature dependence of ionic dc conductivity of the $0.35Na_2O + 0.65[0.4B_2O_3 + 0.6P_2O_5]$ glass.

mol, yielding a $\delta/\Delta E_0$ ratio of 0.072, a value Bischoff has reported as common for an alkali oxide glass.[44] From eq 5, the temperature-dependent activation energy, ΔE, can have values ranging from 94.3 to 65 kJ/mol over the temperature range of −100 to 300 °C. These values are in good agreement with the single activation energy, ΔE_a = 65 J/mol, determined by fitting the conductivity data to the simple Arrhenius equation.

Because the ionic conductivity was found to be non-Arrhenius, as suggested by Bischoff et al., we therefore take the values of ΔE_n and ΔE_m to likewise be the averages of the underlying distributions in each of these terms. However, an unambiguous technique to experimentally measure these two activation energies and their distributions independently of one another has so far remained elusive. Therefore, we must rely on theoretical models to calculate estimates of these two (average) energy barriers in terms of experimentally measurable quantities. It is to these models that we now turn our attention.

3.2. Anderson−Stuart Model. *3.2.1. Theory.* Although several models exist for the calculation of the activation energy, ΔE_a, for ionic conduction in oxide glasses, the Anderson Stuart (A−S) model is the most easily related to the accepted definition of the ionic conductivity, as discussed above, $\sigma = nZe\mu$. On the basis of the ideas of ionic crystal theory and elasticity theory, Anderson and Stuart[36] proposed that the activation energy consisted of two parts, the binding energy and the strain energy, eq 6 below. Their binding energy

$$E_b = -\left(1 - \frac{1}{m}\right)ME_c \tag{6}$$

is assigned to the difference in the columbic energy, $E_c(x) = ((Z_1Z_2e^2)/(\varepsilon_\infty x))$, acting at over a distance x between two point charges, Z_1e and Z_2e, through a dielectric media with dielectric permittivity, ε_∞, of the ion when it is at an equilibrium site and when it is at the halfway point between equilibrium sites for all ion pairs; see Figure 7. In eq 6, M is the Madelung constant for the particular glass structure and represents the summation of the effects from other charges (ions) in the network. The constant m describes the exponent on the repulsive part of the potential for the close approach of ions in the glass. A−S defined the halfway point as half of the jump distance, which was taken to equal half of the lattice constant of the crystal, λ; see Figure 7A. By defining the halfway point with a value, λ, rather than a point, such as x, confusion has arisen as the definition of jump distance has

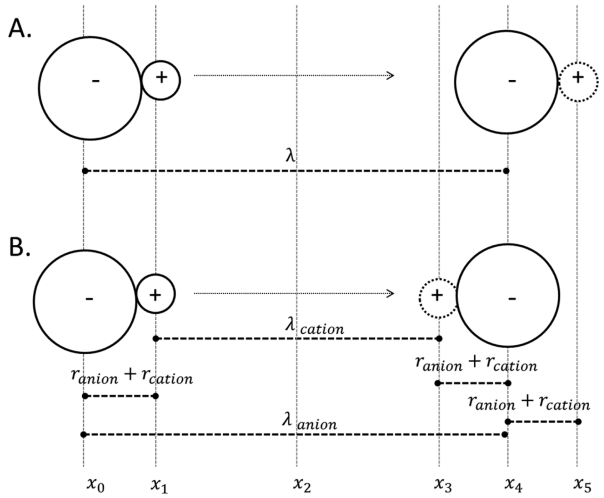

Figure 7. (A) Physical representation of A−S's glass structure, based on a crystal lattice. (B) Physical representation of how the jump distances are calculated based on the physical representation of Martin et al.[45]

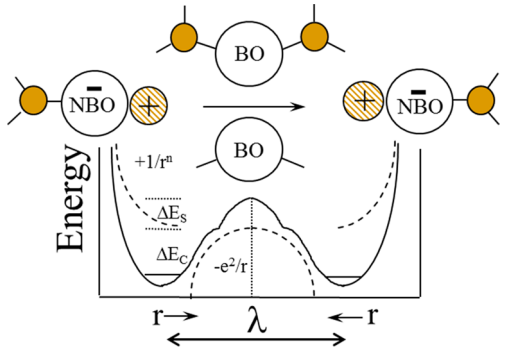

Figure 8. Physical representation of the energetics of ion conduction according to the A−S model by Martin et al.[45]

changed. A more physical, noncrystalline, view of the structure was proposed by Martin et al.;[45] see Figure 8. This representation has been duplicated in Figure 7B, for ease of comparison. As can be seen in Figure 7, the jump distance as defined by A−S is not equivalent to the jump distance as defined by Martin.[45] Therefore, by treating the cation and anion as point charges, with an origin point at x_0 = 0, then we have defined the halfway point as x_2. We may then define the change in columbic energy as the cation travels from point x_1 to point x_2 as $\Delta E_c = E_c(x_2) - E_c(x_1)$. Using experimentally determined ionic radii and cation-to-cation distances, the x points may be defined as $x_1 = r_{anion} + r_{cation}$ and $x_2 = r_{anion} + r_{cation} + \lambda_{cation} = \lambda_{anion}/2$. In the glass system under study here, the Na^+ ion is the cation and the nonbridging oxygen (NBO), O^-, is the anion, so $x_1 = r_O + r_{Na}$ and $x_2 = r_O + r_{Na} + \lambda_{Na}$.

The network strain energy, ΔE_s, was taken by A−S to describe the elastic energy needed to dilate a spherical cavity as the structure deforms to allow the ion to move between sites. The radius of this space before dilation out to the radius of the mobile cation, r_{cation}, is termed the doorway radius, r_D. Typically, it is the case that $r_D < r_{cation}$ and making the strain energy nonzero and positive, thus, the larger the cation, the larger the strain energy. The total change in activation energy, eq 7, can be represented as seen in eq 8. A−S then simplified the equation, taking $(1 - (1/m))M \approx 1$ and using a

dx.doi.org/10.1021/jp409497z | J. Phys. Chem. B 2013, 117, 16577−16586

displacement factor, β, to create the more recognizable expression in eq 9, shown first in CGS and then in SI units. We will be using the SI unit form in this analysis.

$$\Delta E_a = \Delta E_b + \Delta E_s \tag{7}$$

$$\Delta E_a = -\left(1 - \frac{1}{m}\right)\frac{MZ_{anion}Z_{cation}e^2}{\varepsilon_\infty}\left[\frac{1}{x_2} - \frac{1}{x_1}\right] + 4\pi G r_D (r_{cation} - r_D)^2 (CGS)$$

$$\Delta E_a = \left(1 - \frac{1}{m}\right)\frac{MZ_{anion}Z_{cation}e^2}{4\varepsilon_\infty}\left[\frac{1}{r_{cation} + r_{anion}} - \frac{1}{\lambda_O/2}\right] + 4\pi G r_D (r_{cation} - r_D)^2 (SI) \tag{8}$$

$$\Delta E_a = \frac{\beta Z_{anion}Z_{cation}e^2}{\varepsilon_\infty}\left[\frac{1}{r_{cation} + r_{anion}}\right] + 4\pi G r_D (r_{cation} - r_D)^2 (CGS)$$

$$\Delta E_a = \left(1 - \frac{1}{m}\right)\frac{MZ_{anion}Z_{cation}e^2}{4\varepsilon_\infty}\left[\frac{1}{r_{cation} + r_{anion}} - \frac{1}{\lambda_O/2}\right] + 4\pi G r_D (r_{cation} - r_D)^2 (SI) \tag{9}$$

where G is the shear modulus, r_D is the doorway radius, e is the electron charge, r_{cation} is the ionic radius of the cation, r_{anion} is the ionic radius of the anion, ε is dielectric permittivity, and Z_{cation} and Z_{anion} are the formal charges of the mobile cation and the charge compensating anion, respectively. $\beta = -1 + ((r_{cation} + r_{anion})/(\lambda_{anion}/2))$ is the finite displacement factor or interionic separation, which ranges from x_1 (a situation indicating no jump of the ion has taken place) out to the halfway point between adjacent cation equilibrium positions, x_2; see Figure 7.

McElfresh and Howitt[46] argued that the strain energy calculations of A–S, which calculated the energy needed to enlarge a spherical cavity, did not apply to diffusion of an atom in a solid, as it yielded physically unreasonable values. They proposed that a more appropriate strain energy would be for the enlargement of a cylindrical volume, modifying eqs 6–10, where λ_{cation} is the distance a cation must travel between equilibrium positions. We will use the McElfresh and Howitt model for the purposes of these calculations.

$$\Delta E_a = \frac{\beta Z_{anion}Z_{cation}e^2}{4\pi\varepsilon_\infty}\left[\frac{1}{r_{cation} + r_{anion}}\right] + \pi G (r_{cation} - r_D)^2 \frac{\lambda_{cation}}{2} (SI) \tag{10}$$

3.2.2. Calculation of Parameters. From the description previously given, the parameters needed to calculate the activation energy are G, r_{Na}, r_D, ε_∞, and λ_{cation}. Because of a limited number of shear modulus values reported in the literature for these ternary glasses, we have estimated the shear modulus for our particular glasses by exploiting the similar compositional trends of the shear modulus and the glass-transition temperature, T_g, of glasses. The shear modulus, G, has been shown to track the composition dependence of the T_g of the glass quite closely for a wide variety of oxide glasses, such as alkali silicate, borate, and phosphate glasses. The value for G of the binary end member glass, $0.35Na_2O + 0.65B_2O_3$, was taken from the SciGlass database,[47,48] and an average value of $G = 22.7 \pm 2.3$ GPa was found. T_g, studied in a previous work,[33] of the glasses were converted to fractions, $f_T(x) = (T_g(x))/(T_g\ (x = 1))$ and multiplied by the shear modulus of $0.35Na_2O + 0.65B_2O_3$ glass. The values so obtained for these glasses are shown in Figure 9. As expected from this calculation method, G and T_g

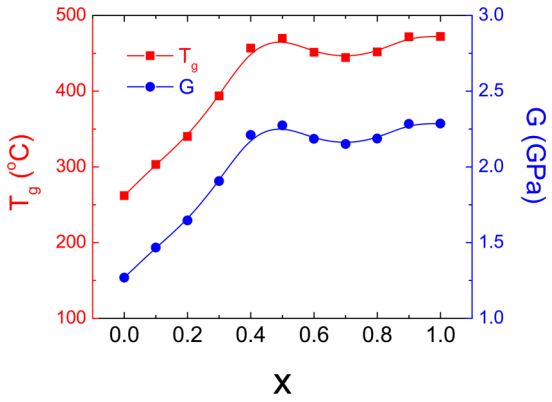

Figure 9. Experimental glass-transition temperature of the $0.35\ Na_2O + 0.65\ [xB_2O_3 + (1 - x)P_2O_5]$ glasses compared with the estimated shear modulus.[52]

track each other directly, with G increasing as T_g increases as P is substituted for B. While G values appear to be unknown for the binary $0.35Na_2O + 0.65P_2O_5$ glass, values for the more common $0.50Na_2O + 0.50P_2O_5$ glass are known, and an average value of ~14 GPa ± 3 GPa is reported.[47,48] The value from the present calculation of the $0.35Na_2O + 65P_2O_5$ glass with a slightly lower T_g value of ~13 GPa is well within the expected range for this glass.

We can calculate an estimate for the doorway radius, r_D, of the glasses using the XRD results by Le Roux et al.[34] on these glasses and the literature results on similar glasses. The diffraction data was then used by Schuch et al.[35] to create a reverse Monte Carlo model that reported Na as having a five-fold oxygen coordination and an average distance between Na-BO and Na-NBO of 2.3 Å. Schuch suggests that oxygen is in a trigonal bipyramidal structure with Na^+ at the center with a five-fold coordination, where the center of each oxygen is 2.3 Å from the center of the Na^+ ion, as seen in Figure 10. It

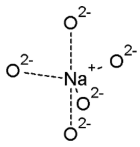

Figure 10. Five-fold coordinated Na^+ in a trigonal bipyramidal structure.

is significant that these Na–O distances appear to be a weak function of the composition in these glasses in that no discernible change in these distances was found across the full compositional range, $0 \le x \le 1$, in these glasses. The literature from Feil et al.[49] reported that $r_{Na} = 0.97$ Å and $r_o = 1.28$ Å in sodium borosilicate glasses. From the geometry of the trigonal bipyramidal structure and the estimated radii of sodium and oxygen, we determined that the largest exit point was in the x–y plane, between two oxygens, with a calculated doorway radius of $r_D = 0.71$ Å. The volumetrically and compositionally dependent jump distance were calculated for

dx.doi.org/10.1021/jp409497z | J. Phys. Chem. B 2013, 117, 16577–16586

the glasses in this study by using the molar volume (see previous study[32]), $r_{cation} = \lambda_{Na} = 2*(((3V_M)/(4\pi))*(N_{Na}/N_{glass})*(1/N_A))^{1/3}$, see Figure 11, where V_M is the molar volume of the glass, N_{Na} is the number of Na ions in one formula unit of the glass, N_{glass} is the total number of ions in one formula unit, and N_A is Avogadro's number.

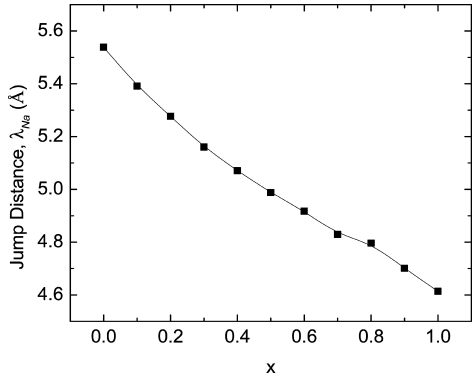

Figure 11. Composition dependence of calculated jump distance between Na^+ sites.

The high-frequency dielectric constant, ε, describes the high-frequency (short time scale) polarizability of the glass structure and decreases the Coulomb binding energy between cations and anions in the glass by reducing the effective electrical field strength between them. In oxide glasses, the ε value is obtained in the high-frequency range that generally lies between $\sim 10^5$ and $\sim 10^{10}$ Hz at temperatures well below the T_g of the glass.[50] We determined the ε values for our glasses between 1 and 10 MHz and at room temperature.

3.2.3. Calculation of the Activation Energy. As seen in Figure 12, the A–S model results in estimates of the activation energy that are slightly larger than the experimentally determined activation energy. Although the calculated activation energy is larger in magnitude, it does have a trend similar, albeit exaggerated, to that of the experimentally measured values. It can also be observed that the binding energy is an order of magnitude larger than the strain energy and is therefore the primary contributor to the overall activation energy.

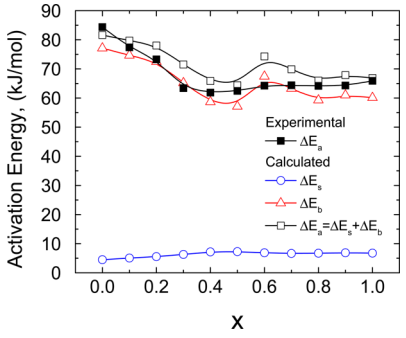

Figure 12. A–S binding energy, the strain energy, and activation energy compared with the experimental activation energy.

3.2.4. Many-Body Effects on the Coulomb Potential. To achieve better agreement with experiment, we have re-examined and evaluated the assumptions made by A–S in their model. Because the binding energy has been shown to dominate the activation energy, its calculation shall be first examined. While A–S first included a Madelung constant term in their calculation of the binding energy, as seen in eq 8, they later dropped it by using the approximate value of β. In doing so, A–S then assumed that the value for the Madelung constant would be less than its value in a cristobalite lattice, $M \leq 1.6$, and that the glass is similar to a heteropolar ionic crystalline lattice, where $m = 9$ to 11. Although such estimates give $(1 - (1/m))M \approx 1.5$, A–S took $(1 - (1/m))M \approx 1$, eliminating the dependence of the activation energy eq 10 on the Madelung constant, and in this way they effectively ignored the obvious and compositionally dependent many-bodied potential effects of nearby charges such as Na^+, O^-, B^{3+}, and P^{5+}. Such effects on the coulomb potential in ionic crystals have long been examined and can be accurately calculated by adding the collective effects of all of the charges at their respective distances. This potential acting collectively on a point charge at a distance r_i in the lattice is given by eq 11 if all of the ion–ion distances r_{ij} are normalized to the nearest neighbor distance, r_0, and the potential maybe rewritten:

$$V_i = \frac{e}{4\pi\varepsilon_0 r_0} \sum_{j \neq i} \frac{Z_j r_0}{r_{ij}} \equiv \frac{e}{4\pi\varepsilon_0 r_0} M_i \qquad (11)$$

This effect generates a Madelung constant for each particular unique ion for each unique crystal structure. Here we are only concerned about the M_{Na^+} value for the mobile cation. Unfortunately, of course, exact values for such Madelung constants for glasses cannot be calculated due to the disordered structure of glass. However, it is also true that given the $1/r$ dependence of the Madelung constant, the local coordination sphere around the mobile cation and out to perhaps the second- and third-coordination spheres would be the dominant terms in the calculation of the M_i values.

By setting the experimental value of the activation energy equal to the calculated activation energy, we can solve for M, the lone adjustable parameter in eq 8. For the purpose of our calculations, we will consider, $m = 10$. As seen in Figure 13,

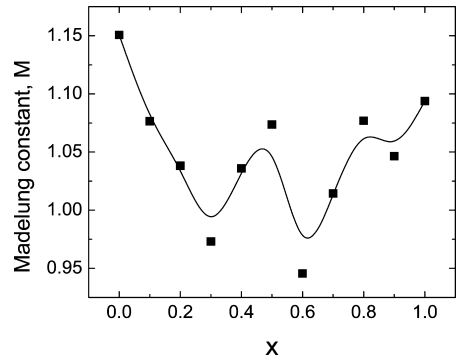

Figure 13. Calculated Madelung constant as it depends on composition.

the Madelung constant would need to vary from a maximum of 1.15 to a minimum of 0.94, a change of only ~10% from an average value of 1.05, c.f. the value of 1 originally proposed by A–S above, to perfectly fit the activation energy data. However, these small adjustments to the M constant result in excellent agreement between our modified A–S model, Figure 14, and the experimentally determined activation energy values. It is to be repeated that there is only a single

dx.doi.org/10.1021/jp409497z | J. Phys. Chem. B 2013, 117, 16577–16586

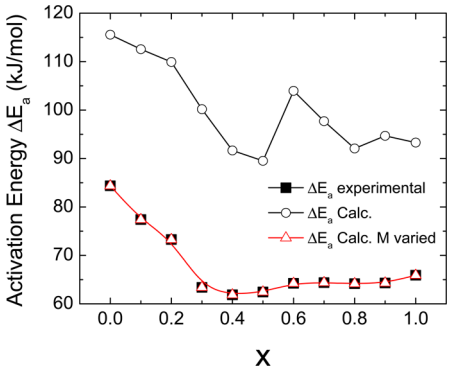

Figure 14. Calculated A–S activation energy with a Madelung constant of 1.6 and variable Madelung constant compared with the experimental activation energy.

adjustable parameter, the M value, in the calculation of the conductivity activation energy, and the total changes to the M value were a maximum of ~10% from an average value of 1.05. Furthermore, it is significant that the changes in the M values follow those of the conductivity activation energy. That is, Figure 13 shows that the M values reach a minimum value in the compositional region where the conductivity activation energies also reach a minimum. Because the M values are a measure of the Coulombic charge density of the glass, higher charge densities at shorter distances tend to increase M, and smaller charge densities and larger distances tend to decrease M, the observed trend of smaller M values in the compositional regions of the minimum in the activation energy are in agreement with the higher mobility, higher conductivity of the mobile Na^+ cations.

3.3. Cause of the Positive MGFE in the Ionic Conductivity. From Figure 12, it is clear that the total activation energy strongly depends on the binding energy. By comparing the trend of the calculated binding energy to the dielectric constant, Figure 15, the strong relationship between

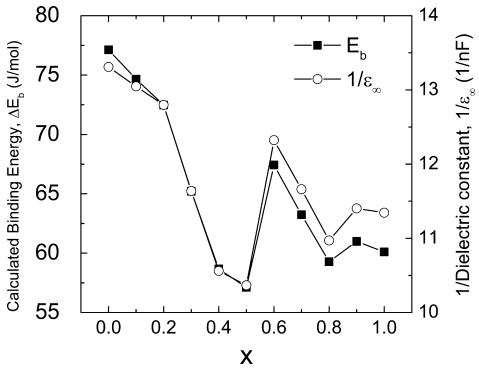

Figure 15. High-frequency dielectric permittivity of the $0.35Na_2O + 0.65[xB_2O_3 + (1 - x)P_2O_5]$ glasses at 30 °C.

them can be observed. This leads to the natural question, "What is the source of the composition dependence of ε_∞?". On close inspection of the results presented so far, the minimum in the conductivity activation energy lies at ~x = 0.4 and is in the same compositional region, where the B^4 fraction has a local maximum in concentration. Therefore, a plausible hypothesis is that the intermediate range order (IRO) in and around the B^4 unit causes the increased ε values and, therefore, the minimum in the activation energy. At 0.1 $\leq x \leq$ 0.4, there are significantly more phosphorus atoms than boron atoms, and our NMR studies have shown a majority of the boron to be in tetrahedral coordination;[51] only a mere 7% of boron are in trigonal configuration at x = 0.4. Therefore, the B^4 unit must bridge to more phosphorus units than boron units, especially at lower x values, where less boron is present. Because P^{5+} has a higher charge density than B^{3+}, P–O–B bonding would tend to polarize the electron cloud around the BO toward phosphorus and thereby decrease the net negative charge density of the B^4 unit. This decreased charge density means the Na^+ ion associated with a B^4 unit would be expected to be less tightly bound due to the smaller effective negative charge on the BO and hence produce a smaller binding energy for the Na^+ ion to hop to the next charge compensation site. It is well known that tetrahedral borons delocalize the single negative charge over the four BOs connected to the B^4 unit. Such charge delocalization and resonance would necessarily increase the average bond distance of Na^+ ions and decrease the negative on the BOs in these glasses and lead to a decreasing columbic binding energy. The added effect here is that in the region of the conductivity activation energy minimum, $x \approx 0.4$, the P^{5+} bonding further reduces the Coulombic binding energy by pulling negative charge away from the BO_4^- groups. These correlations appear to be well-borne out in the data, as Figure 16 shows the composition dependence of the fraction B_4 units

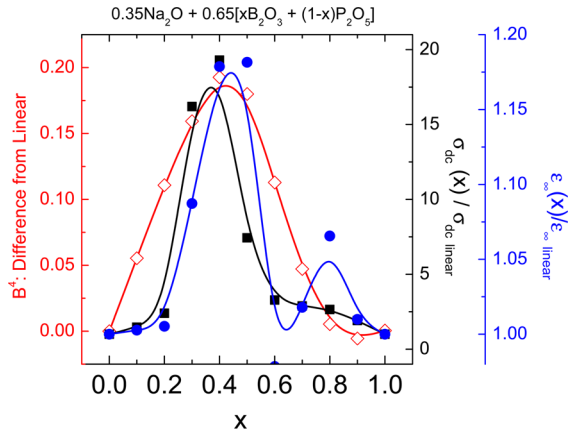

Figure 16. Comparison plot of the scaled fraction of B_4 groups, the scaled high frequency relative dielectric constant, ε_∞, and the scaled dc Na^+ ion conductivity, σ_{dc}.

scaled to a linear trend between 0 for x = 0 and ~0.5 for x = 1, the scaled composition dependence of the relative permittivity to a linear trend between the x = 0 sodium phosphate glass and x = 1 sodium borate glass, and finally the scaled σ_{dc} values, again scaled to the linear trend between the x = 0 and 1 glass. The colocation of the maxima in all three of these quantities lends strong support to the arguments previously developed.

A further and related question is, "How does this explain the maxima in the ε value at glass compositions of x = 0.4 and 0.5 and x = 0.8 in addition to the maxima in ionic conductivity at x = 0.4?". At x = 0.4, B^4 makes up 37% of the SRO structural units and at x = 0.5 B^4 makes up 40% of the SRO structural units according to our previously reported NMR data.[51] However, at x = 0.4 and 0.5, phosphorus units make up 60 and 50% of the SRO units. The NMR data indicate that the number of B_P^4 is greater than the B_B^4 until x =

dx.doi.org/10.1021/jp409497z | J. Phys. Chem. B 2013, 117, 16577–16586

0.4, after which B_B^4 is the dominant boron tetrahedral unit. So the maximum in conductivity occurs where there is the greatest number of B_P^4.

To understand the maximum at $x = 0.8$, we must consider the changes in SRO with x. As x increases, the number of B^4−O−P bridges decreases, but the number of $P^2_{B^4}$ and $P^1_{B^4}$ units increases. If we say that $[P^2]^{-1}$ and $[P^1]^{-2}$ are more basic than $[P^3]^0$, then as they bridge to B, their Na−NBO bond increase in strength.[23] However, the $B^4_{P^2}$ or $B^4_{P^1}$ bonds to Na^+ would be weaker than $B^4_{P^3}$. Therefore, even though B^4 units are now bridging to fewer phosphorus, the phosphorus units are more basic, allowing a decreased activation energy and therefore an increased ionic conductivity.

4. CONCLUSIONS

The strong positive MGFE observed in the ionic conductivity of $0.35Na_2O + 0.65[xB_2O_3 + (1 - x)P_2O_5]$ glasses arises from the negative MGFE in activation energy with changing composition. The composition dependence of the activation energy in these ternary glasses was explained though the Anderson−Stuart Model, which suggested that the columbic binding energy is much greater than the strain energy. The composition dependence of the columbic binding energy was attributed to the composition dependence of the dielectric constant, ε. A maximum in ε was observed at $x \approx 0.4$ and is at a composition where there are a maximum number of B^4 units that can still be completely coordinated by BOs to only phosphorus atoms. The higher charge density, more electronegative P^{5+} is proposed to pull charge away from the already delocalized charge on the BO_4^{-1} groups to create even more delocalized charges and thereby further weaken the columbic forces between the mobile Na^+ ions and the bound negative charges of the borophosphate polyanions. This weakening of the columbic interaction in turn is thought to produce the minimum in the activation energy and produce the maximum in the Na^+ ion conductivity.

AUTHOR INFORMATION

Corresponding Author

*Phone: (515) 294-0745. Fax: (515) 294-5444. E-mail: swmartin@iastate.edu.

Present Address

[†]R.C.: Department of Chemistry University of Manitoba, Manitoba, Canada, R3T N2N.

Notes

The authors declare no competing financial interest.

ACKNOWLEDGMENTS

This research was supported by the National Science Foundation under grant number DMR-0710564 and this research support is gratefully acknowledged. The authors would like to thank Christian Bischoff for his interest and valuable contributions to this paper.

REFERENCES

(1) Storek, M.; Boehmer, R.; Martin, S. W.; Larink, D.; Eckert, H. NMR and conductivity studies of the mixed glass former effect in lithium borophosphate glasses. *J. Chem. Phys.* **2012**, *137*, 124507/124501−124507/124512.

(2) Larink, D.; Eckert, H.; Reichert, M.; Martin, S. W. Mixed Network Former Effect in Ion-Conducting Alkali Borophosphate Glasses: Structure/Property Correlations in the System $[M_2O]1/3[(B_2O_3)x(P_2O_5)1\text{-}x]2/3$ (M = Li, K, Cs). *J. Phys. Chem. C* **2012**, *116*, 26162−26176.

(3) Yao, W.; Martin, S. W. Ionic conductivity of glasses in the MI + M_2S + $(0.1Ga_2S_3 + 0.9GeS_2)$ system (M = Li, Na, K and Cs). *Solid State Ionics.* **2008**, *178*, 1777−1784.

(4) Kim, Y.; Saienga, J.; Martin, S. W. Anomalous Ionic Conductivity Increase in Li_2S + GeS_2 + GeO_2 Glasses. *J. Phys. Chem. B* **2006**, *110*, 16318−16325.

(5) Foix, D.; Martinez, H.; Pradel, A.; Ribes, M.; Gonbeau, D. XPS valence band spectra and theoretical calculations for investigations on thiogermanate and thiosilicate glasses. *Chem. Phys.* **2006**, *323*, 606−616.

(6) Martin, S. W.; Borsa, F.; Svare, I. Distribution of activation energies treatment of fast ion motions in glass. *Proc. - Electrochem. Soc.* **2001**, *2000−32*, 66−78.

(7) Martin, S. W. Ionic conduction in phosphate glasses. *J. Am. Ceram. Soc.* **1991**, *74*, 1767−1784.

(8) Agarwal, A.; Seth, V. P.; Gahlot, P. S.; Khasa, S.; Arora, M.; Gupta, S. K. Study of electron paramagnetic resonance, optical transmission and dc conductivity of vanadyl doped $Bi_2O_3{\cdot}B_2O_3{\cdot}Li_2O$ glasses. *J. Alloys Compd.* **2004**, *377*, 225−231.

(9) Pradel, A.; Kuwata, N.; Ribes, M. Ion transport and structure in chalcogenide glasses. *J. Phys.: Condens. Matter* **2003**, *15*, S1561−S1571.

(10) Pradel, A.; Rau, C.; Bittencourt, D.; Armand, P.; Philippot, E.; Ribes, M. Mixed Glass Former Effect in the System $0.3Li_2S\text{-}0.7[(1\text{-}x)SiS_2\text{-}xGeS_2]$: A Structural Explanation. *Chem. Mater.* **1998**, *10*, 2162−2166.

(11) Prasad, P. S. S.; Rani, A. N. D.; Radhakrishna, S. Mixed glass former effect in silver iodide-silver oxide-boron oxide-arsenic oxide (mol% 66.67 AgI-24.66 Ag_2O-8.33(1-x) B_2O_3-x As_2O_3) quaternary amorphous solid electrolytes. *Solid State Commun.* **1991**, *77*, 967−971.

(12) Prasad, P. S. S.; Rani, A. N. D.; Radhakrishna, S. Mixed glass former effect in silver iodide-silver oxide-vanadium pentoxide phosphorus pentoxide quaternary amorphous solid electrolytes. *Mater. Chem. Phys.* **1990**, *25*, 487−499.

(13) Salodkar, R. V.; Deshpande, V. K.; Singh, K. Enhancement of the ionic conductivity of lithium borophosphate glass: a mixed glass former approach. *J. Power Sources.* **1989**, *25*, 257−263.

(14) Jamal, M.; Venugopal, G.; Shareefuddin, M.; Narasimha Chary, M. Sodium ion conducting glasses with mixed glass formers NaI-Na_2O-V_2O_5-B_2O_3: application to solid state battery. *Mater. Lett.* **1999**, *39*, 28−32.

(15) Zielniok, D.; Cramer, C.; Eckert, H. Structure/property correlations in ion-conducting mixed-network former glasses: Solid-state NMR studies of the system $Na_2O\text{-}B_2O_3\text{-}P_2O_5$. *Chem. Mater.* **2007**, *19*, 3162−3170.

(16) Kim, Y.; Saienga, J.; Martin Steve, W. Anomalous ionic conductivity increase in Li_2S + GeS_2 + GeO_2 glasses. *J. Phys. Chem. B* **2006**, *110*, 16318−16325.

(17) Gedam, R. S.; Deshpande, V. K. An anomalous enhancement in the electrical conductivity of Li_2O: B_2O_3: Al_2O_3 glasses. *Solid State Ionics* **2006**, *177*, 2589−2592.

(18) Taylor, P. C.; Friebele, E. J. Nature of Unique Boron Sites in Borate Glasses. *J. Non-Cryst. Solids.* **1974**, *16*, 375−386.

(19) Prabaker, S.; Rao, K. J.; Rao, C. N. R. 11B NMR Spectra and Structure of Boric Oxide and Alkali Borate Glasses. *Proc. R. Soc. London* **1990**, *429*, 1−15.

(20) Jellison, G. E.; Bray, P. J. Structural Interpretation of B-10 and B-11 Nmr-Spectra in Sodium Borate Glasses. *J. Non-Cryst. Solids.* **1978**, *29*, 187−206.

(21) Elbers, S.; Strojek, W.; Koudelka, L.; Eckert, H. Site connectivities in silver borophosphate glasses: new results from B-11{P-31} and P-31{B-11} rotational echo double resonance NMR spectroscopy. *Solid State Nucl. Magn. Reson.* **2005**, *27*, 65−76.

(22) Bray, P. J.; Geissberger, A. E.; Bucholtz, F.; Harris, I. A. Glass Structure. *J. Non-Cryst. Solids.* **1982**, *52*, 45−66.

(23) Brow, R. K. Review: the structure of simple phosphate glasses. *J. Non-Cryst. Solids.* **2000**, *263*, 1−28.
(24) Martin, S. W. Review of the Structures of Phosphate-Glasses. *J. Solid State Inorg. Chem.* **1991**, *28*, 163−205.
(25) Brow, R. K.; Kirkpatrick, R. J.; Turner, G. L. The Short-Range Structure of Sodium-Phosphate Glasses 0.1. Mas Nmr-Studies. *J. Non-Cryst. Solids.* **1990**, *116*, 39−45.
(26) Sato, R. K.; Kirkpatrick, R. J.; Brow, R. K. Structure of Li,Na Metaphosphate Glasses by P-31 and Na-23 Mas-Nmr Correlated with the Mixed Alkali Effect. *J. Non-Cryst. Solids.* **1992**, *143*, 257−264.
(27) Villa, M.; Scagliotti, M.; Chiodelli, G. Short range order in the network of the borophosphate glasses: a phosphorus-31 NMR-MAS (magic angle spinning) study. *J. Non-Cryst. Solids.* **1987**, *94*, 101−121.
(28) Koudelka, L.; Mosner, P.; Zeyer, M.; Jager, C. Structure and properties of mixed sodium-lead borophosphate glasses. *J. Non-Cryst. Solids.* **2005**, *351*, 1039−1045.
(29) Zeyer-Dusterer, M.; Montagne, L.; Palavit, G.; Jager, C. Combined O-17 NMR and B-11-P-31 double resonance NMR studies of sodium borophosphate glasses. *Solid State Nucl. Magn. Reson.* **2005**, *27*, 50−64.
(30) Qiu, D.; Guerry, P.; Ahmed, I.; Pickup, D. M.; Carta, D.; Knowles, J. C.; Smith, M. E.; Newport, R. J. A high-energy X-ray diffraction, P-31 and B-11 solid-state NMR study of the structure of aged sodium borophosphate glasses. *Mater. Chem. Phys.* **2008**, *111*, 455−462.
(31) Christensen, R.; Olson, G.; Martin, S. W. Structural studies of mixed glass former $0.35Na_2O + 0.65[xB_2O_3 + (1 - x)P_2O_5]$ glasses by Raman and ^{11}B and ^{31}P magic angle spinning nuclear magnetic resonance spectroscopies. *J. Phys. Chem. B* **2013**, *117*, 2169−2179.
(32) Christensen, R.; Byer, J.; Olson, G.; Martin, S. W. The densities of mixed glass former $0.35\ Na_2O+0.65\ [xB_2O_3+(1-x)P_2O_5]$ glasses related to the atomic fractions and volumes of short range structures. *J. Non-Cryst. Solids.* **2012**, *358*, 583−589.
(33) Christensen, R.; Byer, J.; Olson, G.; Martin, S. W. The glass transition temperature of mixed glass former $0.35Na_2O+0.65-[xB_2O_3+(1-x)P_2O_5]$ glasses. *J. Non-Cryst. Solids* **2012**, *358*, 826−831.
(34) Le Roux, S.; Martin, S.; Christensen, R.; Ren, Y.; Petkov, V. Three-dimensional structure of multicomponent $(Na_2O)0.35[(P_2O_5)-1-x(B_2O_3)x]0.65$ glasses by high-energy X-ray diffraction and constrained reverse Monte Carlo simulations. *J. Phys.: Condens. Matter.* **2011**, *23*, 035403/035401−035403/035410.
(35) Schuch, M.; Christensen, R.; Trott, C.; Maass, P.; Martin, S. W. Investigation of the Structures of Sodium Borophosphate Glasses by Reverse Monte Carlo Modeling to Examine the Origins of the Mixed Glass Former Effect. *J. Phys. Chem. C* **2012**, *116*, 1503−1511.
(36) Anderson, O. L.; Stuart, D. A. Calculation of activation energy of ionic conductivity in silica glasses by classical methods. *J. Am. Ceram. Soc.* **1954**, *37*, 573−580.
(37) Murugavel, S.; Vaid, C.; Bhadram, V. S.; Narayana, C. Ion Transport Mechanism in Glasses: Non-Arrhenius Conductivity and Nonuniversal Features. *J. Phys. Chem. B* **2010**, *114*, 13381−13385.
(38) Murugavel, S. Origin of non-Arrhenius conductivity in fast ion conducting glasses. *Phys. Rev. B: Condens. Matter Mater. Phys.* **2005**, *72*, 134204/134201−134204/134205.
(39) Kuwata, N.; Saito, T.; Tatsumisago, M.; Minami, T.; Kawamura, J. Non-Arrhenius ionic conductivity in α-AgI-stabilized composites and rapid quenched glasses. *Solid State Ionics* **2004**, *175*, 679−682.
(40) Kincs, J.; Martin, S. W. Non-Arrhenius conductivity in glass: mobility and conductivity saturation effects. *Phys. Rev. Lett.* **1996**, *76*, 70−73.
(41) Meyer, B.; Borsa, F.; Martin, D. M.; Martin, S. W. NMR spin-lattice relaxation and ionic conductivity in lithium thioborogermanate fast-ion-conducting glasses. *Phys. Rev. B: Condens. Matter Mater. Phys.* **2005**, *72*, 144301/144301−144301/144313.
(42) Mei, Q.; Meyer, B.; Martin, D.; Martin, S. W. Ion trapping model and the non-Arrhenius ionic conductivity in fast ion conducting glasses. *Solid State Ionics* **2004**, *168*, 75−85.
(43) Ribes, M.; Taillades, G.; Pradel, A. Non-Arrhenius conductivity in glassy and crystallized fast ion conductors. A manifestation of cationic disorder. *Solid State Ionics* **1998**, *105*, 159−165.
(44) Bischoff, C.; Schuller, K.; Beckman, S. P.; Martin, S. W. Non-Arrhenius Ionic Conductivities in Glasses due to a Distribution of Activation Energies. *Phys. Rev. Lett.* **2012**, *109*, 075901-1−075901-4.
(45) Martin, S. W.; Angell, C. A. Dc and ac conductivity in wide composition range $Li_2O{\cdot}P_2O_5$ glasses. *J. Non-Cryst. Solids.* **1986**, *83*, 185−207.
(46) McElfresh, D. K.; Howitt, D. G. Activation enthalpy for diffusion in glass. *J. Am. Ceram. Soc.* **1986**, *69*, C237−C238.
(47) Kodama, M.; Ono, A.; Kojima, S.; Feller, S. A.; Affatigato, M. Borate anomaly and anharmonicity in sodium borate glasses. *Phys. Chem. Glasses* **2006**, *47*, 465−470.
(48) Takahashi, K.; Osaka, A.; Furuno, R. The elastic properties of the glasses in the systems R_2O-boron oxide-silicon dioxide (R = sodium and potassium) and sodium oxide-boron oxide. *Yogyo Kyokaishi* **1983**, *91*, 199−205.
(49) Feil, D.; Feller, S. The density of sodium borosilicate glasses related to atomic arrangements. *J. Non-Cryst. Solids.* **1990**, *119*, 103−111.
(50) Liu, L. Space charge and induced dipole relaxation in solid electrolytes. *Solid State Ionics* **1996**, *85*, 25−35.
(51) Christensen, R.; Olson, G.; Martin, S. W. Structural Studies of Mixed Glass Former $0.35Na_2O + 0.65[xB_2O_3 + (1 - x)P_2O_5]$ Glasses by Raman and ^{11}B and ^{31}P Magic Angle Spinning Nuclear Magnetic Resonance Spectroscopies. *J. Phys. Chem. B* **2013**, *117*, 2169−2179.
(52) Christensen, R.; Byer, J.; Olson, G.; Martin, S. W. Glass Transition Temperature of Mixed Glass Former $0.35Na_2O + 0.65[xB_2O_3 + (1-x)P_2O_5]$ Glasses. *J. Non-Cryst. Solids* **2012**, *358*, 826−831.